Vietnam Journal of Mathematics manuscript No.
(will be inserted by the editor)

Minimal Surface Convex Hulls of Spheres

Josef Kallrath and Markus Frey

Received: date / Accepted: date

Abstract We present and solve a new computational geometry optimization problem. Spheres with given radii should be arranged such that a) they do not overlap and b) the surface area of the boundary of the convex hull enclosing the spheres is minimized. An additional constraint could be to fit the spheres into a specified geometry, *e.g.*, a rectangular solid. To tackle the problem, we derive closed non-convex NLP models for this sphere arrangement or sphere packing problem. For two spheres, we prove that the minimal area of the boundary of the convex hull is identical to the sum of the surface areas of the two spheres. For special configurations of spheres we provide theoretical insights and we compute analytically minimal area configurations. Numerically, we have solved problems containing up to 200 spheres.

Keywords Packing problem · convex hull minimization · isoperimetric inequality · computational geometry · non-convex nonlinear programming · global optimization

1 Introduction

In this paper we address a novel kind of arrangement problem or packing problem: The 3 dimensional (3D) minimal-area convex hull sphere arrangement problem (3D-MACH). In this problem we arrange congruent and non-congruent spheres with given, possibly differing radii in a 3D Euclidean space such that the surface area of the boundary of convex hull hosting the spheres is minimized. We assume that each sphere can be moved freely in space but spheres must not

Josef Kallrath
Am Mahlstein 8
D-67273 Weisenheim am Berg, Germany
E-mail: josef.kallrath@web.de

University of Florida, Dept. of Astronomy
Gainesville, FL 32611
E-mail: jkallrath@ufl.edu

· Markus M. Frey
BASF SE, Advanced Business Analytics, G-FSS/OAO
D-67056 Ludwigshafen, Germany
E-mail: markus.mattheaus.frey@basf.com

Technische Universität München, TUM-School of Managment, Munich, Germany
E-mail: markus.frey@tum.de

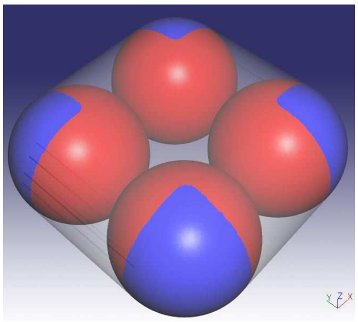

Fig. 1 Square-type arrangement of four equal spheres and illustration of the convex hull. Note that this is not a minimal area arrangement. In 3D, a tetrahedron-type arrangement of spheres minimizes the surface area of the convex hull (see Section 3.3).

overlap; no other restrictions are imposed, except for some selected numerical studies in which we require the spheres to fit into a rectangular solid. A square arrangement of four equal spheres and their convex hull in the 3D Euclidean is depicted in Figure 1.

This problem could be useful in the context of living cells trying to minimize the area surrounding them to the outside world for minimizing the energy loss or surface of attack from the outside world, or molecule configurations to minimize surface tension.

3D-MACH belongs to the class of sphere packing problems in which a given number of congruent or non-congruent spheres have to be packed into a given geometric domain (see [7]). In the closed-packing problem, a set of spheres is arranged in a Euclidean space such that the occupied density of the spheres in space is minimized (*cf.* [19], [23], [26]); for a general overview of sphere packing problems *cf.* [8], [13], or [30]. In contrast to the classical sphere packing problem or the closed-packing problem, we arrange congruent and non-congruent spheres such that the surface area of the boundary of the convex hull is minimized. For spheres with *fixed* center coordinates in a Euclidean space of arbitrary dimension there are some articles about calculating the minimal convex hull, *cf.* [2], [5], [18], or [6]. According to [2], the convex hull in the 3D Euclidean space can even be calculated in polynomial time. However, as the spheres of different radii in the 3D-MACH have to be arranged in space such that we obtain the minimal area convex hull, the problem complexity is established as NP-hard; see Section 3. The 3D-MACH is a natural extension of the minimal perimeter problem of [16] in which discs have to be arranged in a 2D space such the length of the perimeter of the boundary of the convex hull is minimized.

To the best of our knowledge, the present paper contains the first mathematical programming model for the 3D-MACH and provides some theoretical insights into the problem. We will provide analytical solutions for optimal arrangements of small numbers of spheres. Moreover, we will show for up to five spheres, that an optimal arrangement is always reached if the spheres reach the highest number of possible touching points. The paper builds the missing bridge between the field of sphere packing and the field of finding the minimal convex hull for fixed center positions.

A slight modification of the proposed model also allows us to pack spheres into a rectangular solid. From a practical perspective, the rectangular solid could be, for example, a container or the loading area of a truck into which spherical items are to be loaded. The remainder of the paper is structured as follows: In Section 2 we derive the model formulation for the 3D-MACH. Analytic solutions are given in Section 3. Numerical experiments are defined and presented in Section 4. Conclusions in Section 5 complete this paper. Within the paper we use column vectors in $\mathrm{I\!R}^3$, *e.g.*, $\mathbf{x} \in \mathrm{I\!R}^3$, $\mathbf{x}^\mathrm{T}$ refers to the transposed vector of $\mathbf{x}$ and is a row vector, and indices i and j to refer to the spheres involved in the optimization problem.

Among the major contributions of this paper are:

1. the first mathematical programming models for this problem, *i.e.*, closed NLP formulations for 3D-MACH,
2. theoretical insights related to the structure of the minimal-area boundary of the convex hull,
3. analytic solutions for smaller cases and special configurations,
4. polylithic[1] approaches to compute configurations for larger sets of spheres for which the nonlinear and global solvers embedded in the algebraic modeling language `GAMS` (*cf.* [1], [3], [4], or [9]) do not even find feasible points after running several hours.

2 Model Formulation for the 3D-MACH Problem

In this section we derive the mathematical model for the 3D-MACH problem. For ease of reading, the NLP model for computing the boundary of the convex hull is summarized in Section 2.4.

Not only arranging n spheres in $\mathbb{R}^3$ such that the surface area $A(\partial\mathcal{S})$ of the boundary or surface $\partial\mathcal{S}$ of the convex hull $\mathcal{S}$ to be minimized is challenging, but also the construction of $\partial\mathcal{S}$ itself. In general, $\partial\mathcal{S}$ consists of three different types of facets: a) parts of spheres, *i.e.*, spherical polygons with up to $n-1$ vertices, b) triangles in a plane tangent to three spheres, and c) parts of the lateral surface of a cone (circular or elliptic) tangent to two spheres. For four spheres with equal radii arranged 2x2 in the plane, we have two triangles on each side forming a square (see Figure 1). To construct $\partial\mathcal{S}$ we evaluate three ideas or approaches, respectively, and discuss their advantages as well as disadvantages.

2.1 Approach 1: Exploiting the Shadow Property for Spheres with *Fixed* Center Coordinates

Given spheres with radii R_i centered at *known* coordinates $\mathbf{x}_i^0$, we could numerically compute the points on spheres contributing to $\partial\mathcal{S}$ by exploiting the *shadow property*; *cf.* [11] or [17]: Parts of the spheres in the shadow area of light flow from all other spheres are part of the convex hull; see Figure 13 for illustration. Similarly as in modeling the surface of eclipsing binary stars, *cf.* [17] or [28], where the Roche surfaces are subject to the reflection effect, we could cover the surface of the spheres by a grid of approximately uniformly distributed points. If the scalar product of the normal vector of a grid point $\mathbf{x}_1$ on sphere 1 and another grid point $\mathbf{x}_2$ on sphere 2 is negative, *i.e.*, the angle is greater than 90 and less or equal 180, the points have a visual connection or line of light connection them. In such cases, we could eliminate both points, $\mathbf{x}_1$ on $\mathbf{x}_2$, from the overall set of grid points contributing to $\partial\mathcal{S}$. If we would proceed like this for all combinations of points on both spheres, we would obtain a retaining set of points forming those parts of the spheres contributing to $\partial\mathcal{S}$.

For free arrangements of spheres, this approach suffers from the quadratic dependence on both the number of points on spheres *and* on the number of spheres. In addition to the inhibitive numerical effort, it is not clear how to combine this approach with minimizing the surface integral of $\partial\mathcal{S}$, as we have only access to those grid points of spheres contributing to $\partial\mathcal{S}$, but no access to points of $\partial\mathcal{S}$ not belonging to the spheres. Therefore, we have not followed this track further on in this paper.

[1] The term *polylithic* has been coined by Kallrath (2009, [14]; 2011, [15]) to refer to tailor-made modeling and solution approaches to solve optimization problems exploiting several models and their solutions.

2.2 Approach 2: Numerical Grid over a set of Direction Vectors

Using spherical coordinates, we cover the surface of the spheres by a grid of approximately uniformly distributed points with the radial distance from a suitable selected coordinate origin being the most relevant variable describing $\partial\mathcal{S}$. Over the angular index domains θ and φ we generate a grid of direction vectors $\mathbf{m}_{\theta\varphi}$ with center at $\mathbf{x}_{\mathrm{c}}$,

$$\mathbf{x}_{\mathrm{c}} := \frac{1}{\sum_i R_i} \sum_i R_i \mathbf{x}_i^0, \tag{2.1}$$

the averaged radius-weighted center of centers-of-spheres, $\mathbf{x}_i^0$. To each $\mathbf{m}_{\theta\varphi}$ we associate a non-negative variable $r_{\theta\varphi}$ and describe $\partial\mathcal{S}$ based on this spherical coordinates $\mathbf{x} = (r_{\theta\varphi}; \theta, \varphi)$. The $\partial\mathcal{S}$-vector points are subject to the condition that the distance of all spheres's centers $\mathbf{x}_i^0$ is greater or equal to their radii, *i.e.*,

$$\mathbf{n}_{\boldsymbol{\theta\varphi}} \mathbf{x}_i^0 - n^{\mathrm{D}} \geq R_i, \tag{2.2}$$

where the normal vector $\mathbf{n}_{\boldsymbol{\theta\varphi}}$ and origin-distance n^{D} describe the tangential plane at $\mathbf{x}_{\theta\varphi}$, *i.e.*,

$$\mathbf{n}_{\boldsymbol{\theta\varphi}} \mathbf{x}_{\theta\varphi}^{\mathrm{T}} = n^{\mathrm{D}}. \tag{2.3}$$

Note that the angle between $\mathbf{n}_{\boldsymbol{\theta\varphi}}$ and $\mathbf{m}_{\theta\varphi}$ has to be in the range of 90 and 180 degrees, or

$$\mathbf{n}_{\boldsymbol{\theta\varphi}} \mathbf{m}_{\theta\varphi}^{\mathrm{T}} \leq 0, \tag{2.4}$$

i.e., the normal vector of the tangential plane points into the interior of the convex hull. We minimize the surface integral

$$\int_0^\pi \int_0^{2\pi} r_{\theta\varphi}^2 \sin\theta \mathrm{d}\varphi \mathrm{d}\theta,$$

or its discretized version

$$\sum_{\mu=1}^{N_\theta} \left[\sum_{j=1}^{N_\varphi(\theta_\mu)} r_{\theta_\mu\varphi_\nu}^2 \sin\theta_\mu \Delta\varphi(\theta_\mu) \right] \Delta\theta, \tag{2.5}$$

with the number, N_θ of θ-circles θ_μ, and the θ-grid points

$$\theta_\mu := (\mu - 1)\,\Delta\theta, \quad \Delta\theta := \frac{\pi}{N_\theta - 1}.$$

To obtain an approximately uniform distribution of grid points, as in [17], we place $N_\varphi(\theta_\mu)$ equidistant φ-angles on each θ-circles θ_μ, *i.e.*,

$$N_\varphi(\theta_\mu) = 2 \left\lfloor \frac{4}{3} N_\theta \sin\theta_\mu + 1 \right\rfloor,$$

the φ-increments

$$\Delta\varphi(\theta_\mu) := \frac{2\pi}{N_\varphi(\theta_\mu)},$$

and finally, the φ-grid points on the θ-circle θ_μ

$$\varphi_\nu(\theta_\mu) := \left(\nu - \frac{1}{2}\right) \Delta\varphi(\theta_\mu).$$

To keep our non-convex NLP problem computationally tractable, we want to maintain the total number of grid points at a reasonable level of a few hundred points. However, if we want to integrate only the unit sphere, *i.e.*, $r^2_{\theta_\mu\varphi_\nu}$, we need several thousand surface elements to obtain the approximate value of 12.56637 for the exact value of 4π.

The approach has been implemented and works for up to two hundred spheres. We have also implemented and tested Gauß and Chebyshev integration schemes for integration of function over the unit spheres, but they required approximately the same number of grid points and were not better.

2.3 Approach 3: Complete Analytic Representation of the Individual Facets of the Convex Hull Boundary

Analytic representation of $\partial\mathcal{S}$ and its minimal surface would be similar to [16], but so far we have not yet succeeded in transferring these ideas from the 2D to the 3D case as it is not clear how to parameterize the individual facets (parts of spheres, conic bits, and triangles).

2.4 NLP-Model

Approach 2 yields the following intuitive NLP formulation: Consider given spheres $i \in \mathcal{I}$ – we also use index j to refer to spheres – with radii R_i, with $R_i \geq R_j$ if $i > j$. The key variables of the optimization problem are the center coordinates $\mathbf{x}_i^0 = (x_{i1}, x_{i2}, x_{i3})^{\mathrm{T}} \in \mathbb{R}^3$ describing the placing of the spheres. Depending on the needs and situations in which we use the NLP model, we introduce two coordinate frameworks. The first one uses only the positive octant with vectors $\mathbf{x} \in \mathbb{R}^3$, $\mathbf{x} \geq \mathbf{0}$, while in coordinate framework 2 we do not use the non-negativity constraint but require that the sum of weighted distances from the center, $\mathbf{x}_{\mathrm{c}}$,

$$\mathbf{x}_{\mathrm{c}} := \frac{1}{\sum_i R_i} \sum_i R_i \mathbf{x}_i^0 \tag{2.6}$$

of centers $\mathbf{x}_i^0$ of spheres is identical to the origin of the coordinate system, *i.e.*, we fix $\mathbf{x}_{\mathrm{c}} = 0$. In coordinate framework 1, the center variables $\mathbf{x}_i^0$ are subject to the lower bounds

$$x_{id}^0 \geq R_i, \quad \forall \{id\}. \tag{2.7}$$

The non-overlap constraints for spheres i and j read

$$\left(\mathbf{x}_i^0 - \mathbf{x}_j^0\right)^2 = \sum_{d\in\mathcal{D}} \left(x_{id}^0 - x_{dj}^0\right)^2 \geq D_{ij}^2 := \left(R_i + R_j\right)^2, \quad \forall \{(ij)|i < j\}, \tag{2.8}$$

with radius R_i and decision variable x_{id}^0 modeling the center of sphere i in dimension d. Constraints (2.8) are non-convex constraints (the left hand side constitutes a convex function). Note that for n spheres we have $n(n-1)/2$ inequalities of (2.8).

To the grid of direction vectors $\mathbf{m}_{\theta\varphi}$ with center at $\mathbf{x}_c$, the average position of all sphere centers, we seek the values of the non-negative variables $r_{\theta\varphi}$ describing the boundary, $\partial\mathcal{S}$, of the convex hull based on the spherical coordinates $\mathbf{x} = (r_{\theta\varphi}; \theta, \varphi)$. The convex hull vector points are subject to the condition that their distance to all spheres's centers $\mathbf{x}_i^0$ is greater or equal to their radii, *i.e.*,

$$\mathbf{n}_{\boldsymbol{\theta\varphi}} \mathbf{x}_i^0 - n^{\mathrm{D}} \geq R_i, \tag{2.9}$$

where normal vector $\mathbf{n}_{\boldsymbol{\theta\varphi}}$ and origin-distance n^{D} describe the tangential plane at $\mathbf{x}_{\theta\varphi}$, *i.e.*,

$$\mathbf{n}_{\boldsymbol{\theta\varphi}}\mathbf{x}_{\theta\varphi} = n^{\mathrm{D}}. \tag{2.10}$$

The angle between $\mathbf{n}_{\boldsymbol{\theta\varphi}}$ and $\mathbf{m}_{\theta\varphi}$ is forced to be in the range of 90 and 180 degrees, by

$$\mathbf{n}_{\boldsymbol{\theta\varphi}}\mathbf{m}_{\theta\varphi} \le 0. \tag{2.11}$$

We minimize the discretized version of the surface integral

$$\sum_{\mu=1}^{N_\theta}\left[\sum_{\nu=1}^{N_\varphi(\theta_\mu)} r^2_{\theta_\mu\varphi_\nu}\sin\theta_\mu\Delta\varphi(\theta_\mu)\right]\Delta\theta. \tag{2.12}$$

2.5 Symmetry Breaking Constraints

Translational and rotational symmetry is inherent to the problem and makes it very difficult to prove global optimality. If we translate and rotate $\mathcal{S}$, $A(\partial\mathcal{S})$ does not change. We can break translational symmetry, for instance, by fixing the largest sphere, the first or any other sphere, or the center-of-centers. However, some care is needed if we place the spheres only in the first octant of the coordinate system, or within a rectangular box.

Breaking rotational symmetry is more difficult as we can rotate $\mathcal{S}$ over all 4π directions. If we had no restrictions on where to arrange the spheres in the coordinate space, we could fix sphere 1 and request that sphere 2 is placed on a fixed line with its origin in the center of sphere 1 and pointing to a fixed direction.

3 Structural Properties and Analytic Solutions

Here we compile various theoretical and analytic results, among them complexity analysis, isoperimetric inequalties, center coordinates $\mathbf{x}_i^0$, area $A(\partial\mathcal{S})$ of $\partial\mathcal{S}$, or volume, $V(\mathcal{S})$, of $\mathcal{S}$.

To begin with, we cannot expect that minimizing $A(\partial\mathcal{S})$ and minimizing the volume, $V(\mathcal{S})$, of $\mathcal{S}$ will in general give the same arrangement of spheres. For the 2D case, in [16] we have provided an example that demonstrated this. For the 3D case, we have not yet found a case which has minimal $V(\mathcal{S})$ but not minimal $A(\partial\mathcal{S})$, but the following thought experiment indicates that configurations should exist leading to minimal $V(\mathcal{S})$ but not necessarily to minimal $A(\partial\mathcal{S})$. Assume a very large number, say, 10^{23} of tiny spheres with all equal radius R, say, 10^{-23}. Large and tiny in this context means so many tiny spheres that the minimal volume V is essentially independent on whether we prescribe the domain of this volume as a sphere or a cube, *i.e.*, we have so many spheres that boundary effects do not play a role. If the domain is a cube, we get the side length a of that equivalent-volume cube as

$$a = V^{1/3},$$

if it is a sphere, we get its radius r as

$$r = \left(\frac{3V}{4\pi}\right)^{1/3}.$$

Thus, the convex hull is the cube with side a or the sphere with radius r, both leading to minimal $V(\mathcal{S})$. However, while the volume for both configurations is the same, the area is not. The cube area is

$$A_{\mathrm{c}} = 6a^2 = 6V^{2/3},$$

while the surface of the equivalent-volume sphere is

$$A_{\mathrm{s}} = 4\pi r^2 = \sqrt[3]{36\pi} V^{2/3} \simeq 4.836 \cdot V^{2/3}.$$

Thus we have two arrangements with the same minimal volume convex hull with significant difference in the surface area of the convex hull.

The formal justification for the difference of minimizing the $A(\partial\mathcal{S})$, and minimizing $V(\mathcal{S})$ is provided by the isoperimetric inequality

$$V \leq \frac{1}{6\sqrt{\pi}} A^{3/2} \tag{3.13}$$

in $\mathbb{R}^3$; *cf.* [12], Formula (1). If r_* denotes the radius of the largest spheres inscribed in $\mathcal{S}$, we have the tighter inequality proven by [12], formula (3):

$$A^3 - 36\pi V^2 \geq \left[\sqrt{A} - 2\sqrt{\pi} r_*\right]^6 ,$$

which is the base of Hadwiger's proof that the inequality becomes an equality if and only if the convex body or convex set is a sphere with radius r_*. Note that we obtain r_* within our grid approach as well.

The *complexity status of sphere packing* is not known for packing n equal spheres, but sphere packing is NP hard for packing n spheres of different radii with the complexity growing in the number of different radii; *cf.* [10]. Solving the 3D-MACH problem is thus also NP hard, as it contains sphere packing with different radii as a subproblem.

Let us now focus on arrangements of spheres leading to minimal $A(\partial\mathcal{S})$. They are obtained if we have maximal contact (see, for instance, the arrangement of four spheres with two larger spheres and two smaller spheres). We prove this formally for two spheres and extend the idea to three and four spheres. For five spheres, we have two subsets of spheres with maximal contact: A *double tetrahedron* formed by spheres (1,2,3,4) and spheres (1,2,3,5) in maximal contact as displayed in Figure 5. A subgroup of configurations for which we derive analytic results are *planar configurations of spheres*, defined as:

Definition: An arrangement of spheres is called *planar* if the centers of all spheres are contained in one plane.

Examples for planar spherical configurations are the configurations $\mathcal{C}_2^{\mathrm{p}}$, $\mathcal{C}_3^{\mathrm{p}}$, or $\mathcal{C}_4^{2\mathrm{x}2}$, and all sausage configurations discussed below (see Fig. 2). The tetrahedral configuration $\mathcal{C}_4^{\mathrm{t}}$ is not planar. In coordinate framework 2, we can easily enforce planar configurations by fixing $x_{i3}^0 = 0$ for all spheres i.

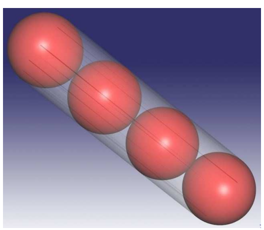

Fig. 2 The sausage configuration for four congruent spheres with radius 1.

An upper bound on the surface of $\partial\mathcal{S}$ for n spheres with radius R follows from the *sausage configuration*, *i.e.*, the spheres are lined-up, are only in contact with the adjacent sphere, and have center coordinates

$$x_{i1}^0 = (2i-1)\,R, \quad i = 1, \ldots, n$$
$$x_{id}^0 = R, \quad i = 1, \ldots, n; \quad d = 2, 3.$$

The convex hull area, A_n^{s}, of this configuration is established by two sphere segments and one cylinder jacket with radius R and length or height, resp., $h = (n-1)2R$

$$A_n^{\mathrm{s}} := 4\pi R^2 + 2\pi R(n-1)2R = 4\pi R^2 n,$$

for all sausage configurations of congruent spheres, the convex hull's area $A(\partial\mathcal{S})$ is identical to the sum of areas of the spheres.

A comparison with the 2D sausage configuration case

$$A_n^{\mathrm{s2}} := 2\pi R + (n-1)2R \leq 2\pi R n$$

shows that the length of the perimeter of the 2D-convex hull is smaller than the sum of the length of perimeters of the circles.

The volume V_n^{s} of sausage configurations with n spheres of radius R is made up of two half-spheres and a cylinder of radius R and height h, *i.e.*,

$$V_n^{\mathrm{s}} = \frac{4}{3}\pi R^3 + \pi R^2\left[(n-1)2R\right] = \frac{4}{3}\pi R^3 \frac{3n-1}{2}.$$

Before we analyze special configurations and their solutions in detail, we formulate the following

Lemma 1: For n spheres with arbitrary radius R, the solid angles contributed by the sphere facets to $\partial\mathcal{S}$ add up to 4π. For n spheres with equal radius R, the surface areas of all partial sphere facets contributed to $\partial\mathcal{S}$ add up to the surface of the full sphere, *i.e.*, $4\pi R^2$.

In [16], we have been able to prove this Lemma for the 2D case. In Appendix B.2.1, we develop the proof for the 3D case for $n < 4$ 3 and symmetric configurations for $n = 4$, and a general proof for any configuration of n spheres based on a generalization of the proof in [16].

3.1 Two Spheres

Let us now consider two spheres with radii R_1 and R_2, $R_1 \geq R_2$ arranged such that their center distance is $d \geq D_{12} = R_1 + R_2$. This configuration, $\mathcal{C}_2^{\mathrm{p}}$, is planar according to the definition above. With the abbreviations

$$\delta := \frac{R_2}{R_1}, \quad \varepsilon := \frac{d - D_{12}}{R_1} = \frac{d - (R_1 + R_2)}{R_1}$$

and exploiting Fig. 3 we obtain, as carried out in Appendix B.1.1, the general results for two spheres

$$A = A(\mathcal{C}_2^{\mathrm{p}}; \varepsilon) = 4\pi R_1^2 \left[1 + \delta^2 + \frac{\varepsilon}{4}\frac{4\delta + \varepsilon + \delta\varepsilon}{1 + \delta + \varepsilon}\right].$$

For small values of ε, the non-negative *detached-correction* term

$$\Delta := \frac{\varepsilon}{4}\frac{4\delta + \varepsilon + \delta\varepsilon}{1 + \delta + \varepsilon}$$

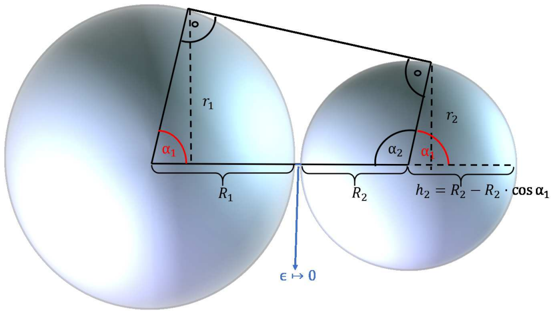

Fig. 3 Two non-touching spheres in the z-x-plane and their basic geometry to derive an analytic expression for the area of $\partial\mathcal{S}$.

approaches zero, while for $\varepsilon \to +\infty$ the term diverges to $+\infty$. As $\Delta \geq 0$, for $\varepsilon = 0$, $A(\partial\mathcal{S})$ takes its minimal value (see Figure 3)

$$A_{2c} = A(\mathcal{C}_2^{\mathrm{p}}; 0) = 4\pi R_1^2 \left[1 + \delta^2\right] = 4\pi R_1^2 + 4\pi R_2^2.$$

This proves our intuitive view that we get the minimal area of $\partial\mathcal{S}$ if the two spheres touch each other (see Fig.3), *i.e.*, they are in contact. Moreover, we can derive the following interesting property of two touching spheres.

Lemma 1 *The surface area, A_{2c}, of the boundary of the convex hull of two touching spheres equals the sum of the areas of both spheres.*

In coordinate framework 1, the center coordinates, $\mathbf{x}_1$ and $\mathbf{x}_2$, of the two spheres are given by

$$\mathbf{x}_1^0 = R_1(1,1,1)^{\mathrm{T}}, \quad \mathbf{x}_2^0 = (2R_1 + R_2, 1, 1)^{\mathrm{T}}.$$

The center-of-centers, $\mathbf{x}_{\mathrm{c}}$, is given by

$$\mathbf{x}_{\mathrm{c}} = (R_1 + R_2, 1, 1)^{\mathrm{T}}.$$

In coordinate framework 2, the center-of-centers is identical to the origin and the center coordinates, $\mathbf{x}_1$ and $\mathbf{x}_2$, of the two spheres are given by

$$\mathbf{x}_1^0 = (-R_2, 0, 0)^{\mathrm{T}}, \quad \mathbf{x}_2^0 = (R_1, 0, 0)^{\mathrm{T}}.$$

3.2 Three Spheres

At first, we consider the planar configuration $\mathcal{C}_3^{\mathrm{p}}$ of three touching spheres with equal radius R: $\partial\mathcal{S}$ is made up by two triangles contributing an area of

$$2 \cdot \frac{1}{2} 2R \cdot \sqrt{3}R = 2\sqrt{3}R^2,$$

three half cylinder jackets adding an area of

$$3 \cdot \frac{1}{2} 2\pi R \cdot 2R = 6\pi R^2,$$

and three partial spheres, by Lemma 1, contributing an area of

$$3 \cdot \frac{1}{3} 4\pi R^2 = 4\pi R^2,$$

$$2 \cdot \frac{1}{2} 2R \cdot \sqrt{3} R + 3 \cdot \frac{1}{2} 2\pi R \cdot 2R + 3 \cdot \frac{1}{3} 4\pi R^2$$

i.e., the total surface area of $\partial\mathcal{S}$ is

$$2R^2 \left[5\pi + \sqrt{3}\right] \approx 11.1\pi R^2 < 4\pi R^2 n, \quad n = 3.$$

Now we consider the general case $\mathcal{C}_3$ of three touching spheres with radii $R_1 \geq R_2 \geq R_3$ (see Fig. 4). We exploit the result of two spheres, that minimal $A(\partial\mathcal{S})$ is obtained when the three spheres are in contact, *i.e.*, the center coordinates are subject to the simultaneous conditions

$$\left(\mathbf{x}_i^0 - \mathbf{x}_j^0\right)^2 = D_{ij}^2, \quad \forall (ij) \in \{(1,2),(1,3),(2,3)\}.$$

Without loss of generality, we fix the z-coordinate $x_{13}, x_{23}, x_{33} = 0$ for all spheres, and the y-coordinate $x_{12}, x_{22} = 0$ for spheres 1 and 2. We further fix $x_{11} = 0$, *i.e.*, spheres 1 is placed at $(0,0,0)$. This leaves us with three unknown variables x_{21}, x_{31}, and x_{22}. If we want to place all spheres in the first octant, we just transform all coordinates to (R_1, R_1, R_1) and obtain the center coordinates of the spheres as derived in Appendix B.1.2

$$\mathbf{x}_1^0 = (x_{11}, x_{12}, x_{13})^{\mathrm{T}} = R_1(1,1,1)^{\mathrm{T}} \tag{3.14}$$

$$\mathbf{x}_2^0 = R_1(2+\rho, 1, 1)^{\mathrm{T}}, \quad \rho := R_2/R_1 \tag{3.15}$$

$$\mathbf{x}_3^0 = \left(R_1 + \frac{R_1R_2 + R_1R_3 - R_2R_3 + R_1^2}{R_1 + R_2}, R_1 + \frac{2\sqrt{(R_1+R_2+R_3)\,R_1R_2R_3}}{R_1+R_2}, R_1\right)^{\mathrm{T}}. \tag{3.16}$$

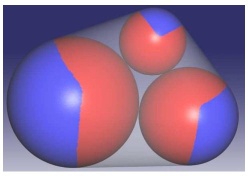

Fig. 4 Optimal arrangement of three non-congruent spheres. In an optimal solution, leading to the minimal area of the surrounding convex hull, the three spheres touch each other.

In the special case of three equal spheres with radius R, we obtain

$$\mathbf{x}_1^0 = R(1,1,1)^{\mathrm{T}} \tag{3.17}$$

$$\mathbf{x}_2^0 = R(3,1,1)^{\mathrm{T}} \tag{3.18}$$

$$\mathbf{x}_3^0 = R\left(2, 1+\sqrt{3}, 1\right)^{\mathrm{T}}. \tag{3.19}$$

3.3 Four Spheres

At first, we consider the planar configuration $\mathcal{C}_4^{2\text{x}2}$ of four spheres with equal radius R arranged as a square (see Fig. 1). The boundary, $\partial\mathcal{S}$, of $\mathcal{S}$ is made up by two squares yielding an area of

$$2 \cdot 4R^2 = 8R^2,$$

four half cylinder jackets adding an area of

$$4 \cdot \frac{1}{2} 2\pi R \cdot 2R = 8\pi R^2,$$

and four partial surfaces of a spheres, by Lemma 1, adding an area of

$$4 \cdot \frac{1}{4} 4\pi R^2 = 4\pi R^2,$$

i.e., the total surface of ∂S is

$$A_{4,2\text{x}2} = 4R^2 \left[3\pi + 2\right] \approx 45.7 < 4\pi R^2 n, \quad n = 4.$$

This result remains valid when we shift the spheres to a rhombus arrangement as displayed in Fig. 5 (a). Note that the volume of $\mathcal{C}_4^{2\text{x}2}$ is given by the volume of a cube, four half cylinders and for quarter spheres, *i.e.*,

$$\begin{aligned} V(\mathcal{S}) &= (2R)^3 + 4 \cdot \frac{1}{2}\pi R^2 2R + 4 \cdot \frac{1}{4}\frac{4}{3}\pi R^3 \\ &= \frac{8}{3}\left(3 + 2\pi\right) R^3. \end{aligned}$$

Second, we consider configuration $\mathcal{C}_4^{\text{t}}$ which consists of four spheres with equal radius R arranged as a regular tetrahedron (see Fig. 5 b):

The derivation exploits the dihedral or face-edge-face angle β of the base area to the sides of a regular tetrahedron, *i.e.*, the angle formed by the intersection of two planes (*cf.* [20])

$$\beta = 2 \arcsin \frac{1}{\sqrt{3}} = \arccos \frac{1}{3} \simeq 70^\circ.52877936,$$

The area A_4^{th} of $\partial\mathcal{S}$ for this tetrahedron configuration consists of four triangles contributing an area of

$$4 \cdot \frac{1}{2} 2R \cdot \sqrt{3}R = 4\sqrt{3}R^2$$

plus six cylinder jackets with arc length $180 - \beta$ leading to an area of

$$6 \cdot \frac{180 - \beta}{360} 2\pi R \cdot 2R = \frac{180 - \beta}{15}\pi R^2 \simeq 7.298\pi R^2$$

plus four quarter-spheres (Lemma 1) contributing an area of

$$4 \cdot \frac{1}{4} 4\pi R^2 = 4\pi R^2,$$

i.e., the total surface, A_4^{th}, of $\partial\mathcal{S}$ is

$$A_4^{\text{th}} = 4R^2 \left[\left(\frac{180 - \beta}{60} + 1 \right) \pi + \sqrt{3} \right] \simeq 42.4222R^2 < 4\pi R^2 n, \quad n = 4.$$

For the volume $V_4^{\rm th}$ consisting of four rectangular solids corresponding to the four triangles, a tetrahedron in in the interior, six partial cylinders and four quarter spheres, we obtain similarly

$$\begin{aligned} V_4^{\rm th} &= 4\cdot\left(\frac{1}{2}2R\cdot\sqrt{3}R\right)\cdot R+\frac{(2R)^3}{6\sqrt{2}}+6\cdot\frac{180-\beta}{360}\pi R^2\cdot 2R+4\cdot\frac{1}{4}\cdot\frac{4}{3}\pi R^3 \\ &= \frac{1}{30}R^3\left(220\pi-\pi\beta+20\sqrt{2}+120\sqrt{3}\right)\simeq 23.524R^3. \end{aligned}$$

while the numerical integrations yields 23.5217.

We compute the center coordinates of four spheres with radii $R_1\geq R_2\geq R_3\geq R_4$ by exploiting the solution of $\mathbf{x}_1^0$, $\mathbf{x}_2^0$, and $\mathbf{x}_3^0$. For convenience, we work with $\mathbf{x}_i^0-(1,1,1)^{\rm T}$, $i=1,2,3$, and obtain the three conditions for sphere 4 and its center coordinates $\mathbf{x}_4^0=(x_{41},x_{42},x_{43})^{\rm T}$:

$$(x_{41}-x_{11})^2+(x_{42}-x_{12})^2+(x_{43}-x_{13})^2=d_{41}^2:=(R_1+R_4)^2$$

$$(x_{41}-x_{21})^2+(x_{42}-x_{22})^2+(x_{43}-x_{23})^2=d_{42}^2:=(R_2+R_4)^2$$

$$(x_{41}-x_{31})^2+(x_{42}-x_{32})^2+(x_{43}-x_{33})^2=d_{43}^2:=(R_3+R_4)^2$$

With the special fixations

$$x_{13},x_{23},x_{33}=x_{12},x_{22}=x_{11}=0$$

we obtain

$$x_{41}=\frac{1}{2x_{21}}\left(d_{41}^2-d_{42}^2\right)$$

$$x_{42}=\frac{1}{2x_{32}}\left[d_{42}^2-d_{43}^2-(x_{41}-x_{21})^2+(x_{41}-x_{31})^2\right]+\frac{1}{2}x_{32}$$

$$x_{43}=\pm\sqrt{d_{41}^2-x_{41}^2\ -x_{41}^2}.$$

Note that we can place sphere 4 *above* or *below* the plane in which the first three spheres are fixed. We continue with only the *above* solution and obtain

$$x_{41}=R_1+\frac{1}{2x_{21}}\left(d_{41}^2-d_{42}^2\right) \tag{3.20}$$

$$x_{42}=R_1+\frac{1}{2x_{32}}\left[d_{42}^2-d_{43}^2-(x_{41}-x_{21})^2+(x_{41}-x_{31})^2\right]+\frac{1}{2}x_{32} \tag{3.21}$$

$$x_{43}=R_1+\sqrt{d_{41}^2-x_{41}^2\ -x_{42}^2} \tag{3.22}$$

after transforming back to coordinate framework 1 with of $\mathbf{x}_1^0$, $\mathbf{x}_2^0$, and $\mathbf{x}_3^0$ as in (3.14) - (3.16). The resulting arrangement is shown in Fig. 5 (c).

As a special case, we get the tetrahedron configuration with four equal spheres of radius R. In coordinate framework 1, the center coordinates are given by

$$\mathbf{x}_1^0=R(1,1,1)^{\rm T},\quad \mathbf{x}_2^0=R(1,1+\sqrt{2},1+\sqrt{2})^{\rm T}$$

$$\mathbf{x}_3^0=R(1+\sqrt{2},1,1+\sqrt{2})^{\rm T},\quad \mathbf{x}_4^0=R(1+\sqrt{2},1+\sqrt{2},1)^{\rm T}.$$

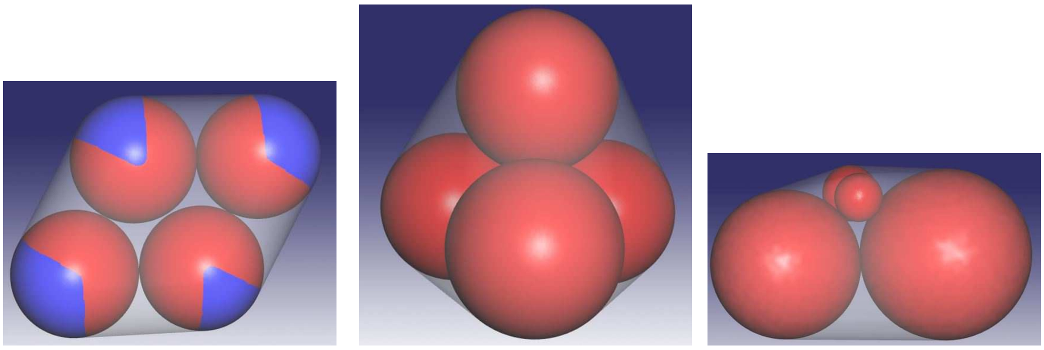

(a) Four congruent spheres arranged as a rhombus

(b) Optimal regular-tetrahedron arrangement of four congruent spheres.

(c) Four non-congruent spheres arranged as an irregular tetrahedron. The three largest spheres are positioned in a plane, and sphere 4 is above this plane.

Fig. 5 Arrangement of four congruent spheres as a rhombus (a), and optimal arrangements as a regular tetrahedron (b), and four non-congruent spheres (c), such that $A(\partial\mathcal{S})$ is minimal.

3.4 Five Spheres

The center coordinates of configuration $\mathcal{C}_5$ of five touching spheres with radii $R_1 \geq R_2 \geq R_3 \geq R_4 \geq R_5$ leading to minimal $A(\partial\mathcal{S})$ are derived similarly as in the case of four spheres, *i.e.*, $\mathbf{x}_1^0$, $\mathbf{x}_2^0$, $\mathbf{x}_3^0$, and $\mathbf{x}_4^0$ are identical to (3.20) - (3.22) while for $\mathbf{x}_5^0$, we use the negative sign in formula (3.22)

$$x_{51} = R_1 + \frac{1}{2x_{21}}\left(d_{51}^2 - d_{52}^2\right) \tag{3.23}$$

$$x_{52} = R_1 + \frac{1}{2x_{32}}\left[d_{52}^2 - d_{53}^2 - (x_{51} - x_{21})^2 + (x_{51} - x_{31})^2\right] + \frac{1}{2}x_{32} \tag{3.24}$$

$$x_{53} = R_1 - \sqrt{d_{51}^2 - x_{51}^2 - x_{52}^2}. \tag{3.25}$$

3.5 General findings

The surface area $A(\partial\mathcal{S})$ for two touching spheres is

$$A = 4\pi R_1^2(1 + \delta^2) = 4\pi R_1^2 + 4\pi R_2^2,$$

i.e., $A(\partial\mathcal{S})$ for two touching spheres is identical to the sum of the surface areas of both spheres. The property

$$A(\partial\mathcal{S}) = \sum_i 4\pi R_i^2$$

is also fulfilled for the sausage configuration of n congruent spheres. In all other configurations and $n > 2$ we observe

$$A(\partial\mathcal{S}) < \sum_i 4\pi R_i^2.$$

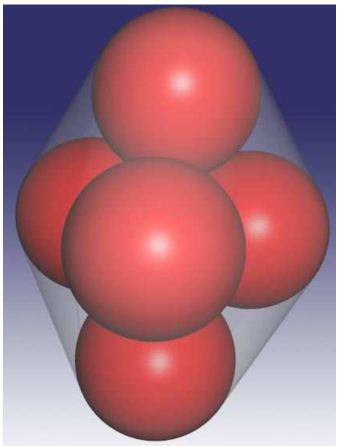

(a) Optimal arrangement of five congruent spheres.

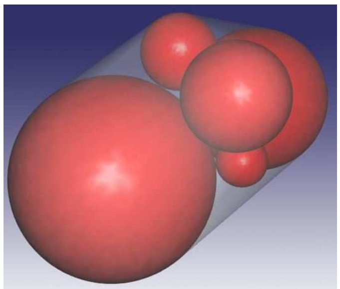

(b) Optimal arrangement of five non-congruent spheres.

Fig. 6 Optimal arrangement of five spheres with equal radius (a) and different radii (b) leading to minimal $A(\partial\mathcal{S})$.

4 Computational insights

In the next section, we show implementation details as well as conducted numerical experiments. First, in Section 4.1 we provide insights how we visualize our sphere arrangements in $\mathbb{R}^3$. In Section 4.2, five experimental setups are presented to solve the problem of arranging spheres. Section 4.3 contains numerical studies. In the last Section 4.4, we wrap up insights produced by the computational experiments.

4.1 Visualization

To display the boundary $\partial\mathcal{S}$ of the convex hull $\mathcal{S}$, we use the QuickHull algorithm by [25] and generate an input file for a 3D viewing program (in the case of this paper `GLC Player 2.3.0` www.glc-player.net). We feed the QuickHull algorithm with the points $\mathbf{x}_{\theta\varphi}$ representing $\partial\mathcal{S}$ as computed by our NLP models (usually, 1,107 grid points), and alternatively, by numerically approximating the surface of the spheres using a Catmull–Clark subdivision (see https://en.wikipedia.org/wiki/Catmull–Clark_subdivision_surface), which divides a dodecahedron several times and in this way approximates a sphere. Establishing $\partial\mathcal{S}$ from our grid points $\mathbf{x}_{\theta\varphi}$, we also obtain an approximate value A^{gP} of $A(\partial\mathcal{S})$. The area based on the dodecahedron division is denoted by A^{sL} (2,761 hull vertices), and A^{sH} with higher resolution (41,755 hull vertices), respectively. Similarly, we denote the volumes V^{gP}, V^{sL}, and V^{sH} of $\mathcal{S}$. We have tuned the resolution by comparison with the analytic solutions in Section 3. For the tetrahedron arrangement and $R=1$, for instance, numerically we obtain $A^{\mathrm{sL}}=42.3979$, $A^{\mathrm{gP}}=42.3155$, and with highest resolution, $A^{\mathrm{sH}}=42.4206$, which differs from the theoretical value of 42.4222 only by 0.37%.

4.2 Experimental setup

The running time limit varies from 15 minutes to 24 hours. We use the global solver `BARON` (*cf.*[27]) using a single core processor. We perform the followings sets of algorithmic experiments:

1. Monolith (M): The NLP problem as it is. We distinguish between the two settings
   (a) Exploiting contact (MT): In (2.8), we use equalities instead of inequalities.
   (b) No contact (MnT): Non-overlap in (2.8) is modeled as greater-or-equal inequalities.
2. Polylithic 1 (P1): A polylithic approach which uses a homotopy approach. At first, we solve the sphere packing problem minimizing the radius or the surface of the sphere hosting all spheres. From this initial arrangement of spheres, we derive initial values for problem `minACH`. We expect this approach to become more efficient when n becomes large.
3. Polylithic 2 (P2): Similar to P1, but this time, we solve the sphere packing problem minimizing the volume of the rectangular box hosting all spheres. From this initial arrangement of spheres, we derive initial values for problem `minACH`.
4. Polylithic 3 (P3): In this approach, initially, we minimize the sum of weighted distances from the center $\mathbf{x}_{\mathrm{c}}$ of spheres' centers $\mathbf{x}_i^0$; see (2.6) for definition. Then, we fix $\mathbf{x}_{\mathrm{c}}$ and $\mathbf{x}_i^0$ and solve the `minACH` problem.
5. Polylithic 4 (P4): Similar to P3, but instead of re-solving after the initial problem allowing the spheres to change their center coordinates, we fix the center coordinates and exploit that, for fixed sphere center coordinates, we can decompose the problem into direction vectors and solve `minACH` for each grid direction $\mathbf{m}_k$ separately. For up to 40 spheres, these individual problems are solved within 5 to 30 seconds yielding an initial solution for $\partial\mathcal{S}$.

After P1, P2, P3, or P4 we relax all variables and try to improve the current solution by solving `minACH`.

The monolith formulation (non-convex NLP) as well as the polylithic approaches P1 – P4 are implemented in `GAMS` 24.9.2. The computations are executed on a 64 bit machine with an Intel(R) Core(TM) i7 CPU 3.33 GHz, 16 GB RAM running Windows 7.

4.3 Numerical study

In this subsection, we report the most interesting findings of our computational study for congruent (see Section 4.3.1), and non-congruent spheres (see Section 4.3.2) as well as the packing of non-congruent spheres in a rectangular solid (see Section 4.3.3).

As an instance identifier we apply a two field notation. Congruent spheres are denoted by Cx where x stands for the number of spheres considered; similarly, we use NCx for non-congruent spheres. To distinguish between instances having the same number of non-congruent spheres but different sphere radii, we additionally label the instance with an alphabetical letter, *e.g.*, NC100a and NC100b.

In the computational study, we use the term global optimum, or global optimality, in the sense of small relative gaps (difference between upper and lower bound divided by the lower bound) of the order of 10^{-5} as numeric solvers dealing with finite number arithmetic are subject to round-off errors. In this sense, all the presented results are only approximations, and although the small gaps hint on (near) optimal results, due to the rounding errors, we do not obtain reliable results in the mathematically strict meaning. For packing circles in a unit square, high precision guaranteed enclosures for both the global optimizer and the global optimum value and details of the interval arithmetic-based core elimination method are presented in a series of publications by Markót and Csendes (2005,[22]) and Markót (2007,[21]). For some instances we have derived analytic solutions. This enables us to evaluate the quality of our numerical solutions independently of the gaps.

4.3.1 Congruent spheres

For spheres with equal radius R, we are able to find feasible solutions for up to 200 spheres. As the value of the radius neither affects the computational complexity nor the resulting arrangement of spheres in the plane, we set the radius to $R = 1$. In Table 1 we report for different instances (Inst) the experimental setup (ES), presented in Section 4.2, leading to the best arrangements found with the area of the surrounding convex hull shown in row $A(\partial S)$.

Inst	C5	C10	C25	C50	C80	C99	C200
ES	P4	P3	P3	P3	P3	P1	P1
$A(\partial S)$	34.8575	80.5739	157.647	265.546	356.138	383.875	704.188

Table 1 Results for congruent spheres. Best experimental setups leading to the smallest $A(\partial S)$ for instances with congruent spheres.

The results reveal that experimental setup P3 outperforms the other setups in most instances for $n < 50$. However, the more spheres are considered in the instance, the better experimental setup P1 performs assuming that the spheres are arranged in a convex hull which itself approaches a sphere. In general, our experiments for spheres support the Lemma from physics that a sufficient number of congruent spheres (or molecules) in nature always arrange spherical, such that minimal $A(\partial \mathcal{S})$ or diameter of $\mathcal{S}$ is reached (*cf.* [29] or [30]). Experimental setup P2, assuming that the spheres arrange rather in a rectangular solid, never performed better than P3 except when using two or three spheres. The resulting arrangements of spheres in Figure 7 for 10, 50, and 99 spheres show that the more spheres are considered, the better the convex hull approximates a sphere.

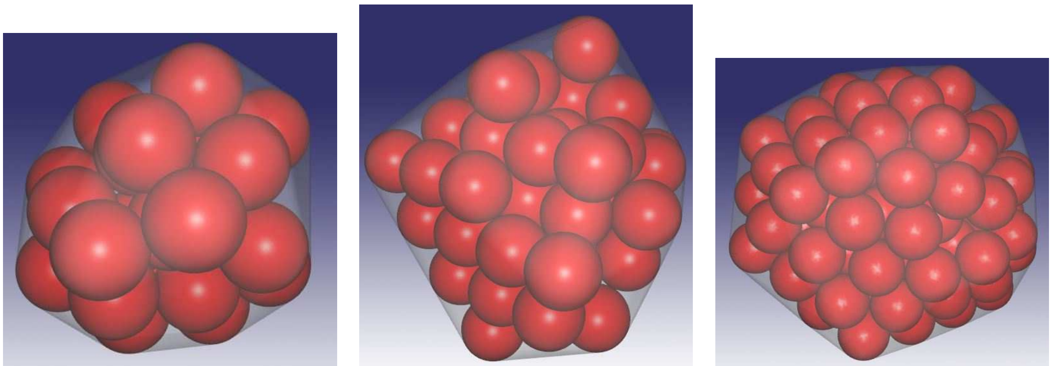

(a) Best obtained arrangement for 25 congruent spheres. (b) Best obtained arrangement for 50 congruent spheres. (c) Best obtained arrangement for 99 congruent spheres.

Fig. 7 Spherical arrangements of congruent spheres for instances C25, C50, and C99. The convex hull approaches a sphere only slowly.

4.3.2 Non-congruent spheres

The decision problem whether the given arrangement of non-congruent spheres is minimal area of the convex hull is NP-hard, in contrast to problems with congruent spheres for which the complexity is not known; *cf.* [10]. The complexity increase for non-congruent spheres is also reflected in our computational experiments: we have been able to solve problems involving up to 200 congruent spheres with unit radius. For non-congruent spheres we have solved problems of up to 200 spheres with some systematic distribution of radii. For example, for one large scale experiment with non-congruent spheres we divide the spheres into two types with different radii. However, beyond a number of 200 spheres, we have difficulties in even finding just feasible points.

In Table 2 we give the arbitrarily specified radii of the spheres in the considered instances. According to Table 3 we obtain the best result with experimental setup P3.

Inst	R
NC3	1.0; 1.5; 2.0
NC4	0.8; 1; 2.5; 3
NC5	0.5; 0.75; 1; 1.5; 2.0
NC6	0.5; 0.75; 1; 1.25; 1.5; 2.0
NC7	1.0; 1.2; 1.4; 1.6; 1.8; 2.0; 3.0
NC8	0.25; 1.0; 1.2; 1.4; 1.6; 1.8; 2.0; 3.0

Table 2 Radii of the non-congruent spheres for the instances NC3 to NC8.

Inst	NC3	NC4	NC5	NC6	NC7	NC8
ES	$P4$	$P3$	$P3$	$P3$	$P3$	$P3$
$A(\partial S)$	194.985	86.8615	96.5994	218.584	218.737	218.758

Table 3 Results for non-congruent instances. For NC3, NC4, and NC5 we have analytic configurations to which we compared our best experimental setups leading to the smallest $A(\partial S)$ for instances with non-congruent spheres. The solution of NC6 is displayed in Figure 14 (b).

The resulting arrangements for instances NC6, NC7, and NC9 are displayed in Figure 8. The obtained arrangements for instances NC3, NC4, and NC5 are similar to those shown in Figure 4, 5 (b) and 6 (b), respectively, and thus are proven to be optimal.

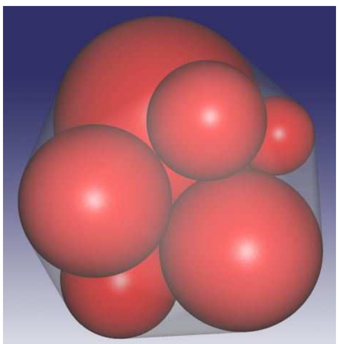
(a) NC6.

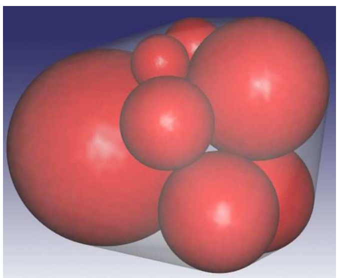
(b) NC7.

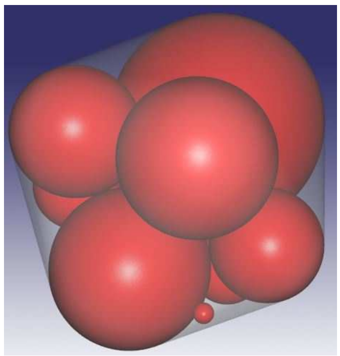
(c) NC8.

Fig. 8 Best obtained arrangements for instances NC6, NC7, and NC8.

To get results for large scale non-congruent instances, we select the radii of the spheres in a systematic way and reduce the number of sphere types with different radii to two. With this instance setup we are able to conduct large scale experiments. In instances NC60, NC120, and NC200a half of the spheres have radius $R = 1$ while the other half has radius $R = 1/2$. Table 4 reports the corresponding results.

Inst	NC60	NC120	NC200a	NC200b
ES	$P3$	$P1$	$P1$	$P1$
$A(\partial S)$	183.0810	289.9942	449.7677	9,557,823
r_{i}	3.53	4.54	5.46	842.53
r_{o}	3.97	4.91	6.21	885.71

Table 4 Results for non-congruent instances. Best experimental setups leading to the smallest $A(\partial\mathcal{S})$ for instances with non-congruent spheres with systematical radii. Note that instance NC200b contains 200 non-congruent spheres with radii $R_i = 201 - i$ and thus has a much larger value of $A(\partial S)$. The radii r_{i} and r_{o} of the inner and outer sphere to $\mathcal{S}$ provide an estimation of how close the convex hull is to a sphere.

Observing the sphere arrangements in Figure 9, we come to Conjecture 1.

Conjecture 1: For large numbers n of spheres with different radii R_i, the convex hull minimizing $A(\partial\mathcal{S})$ approaches a sphere.

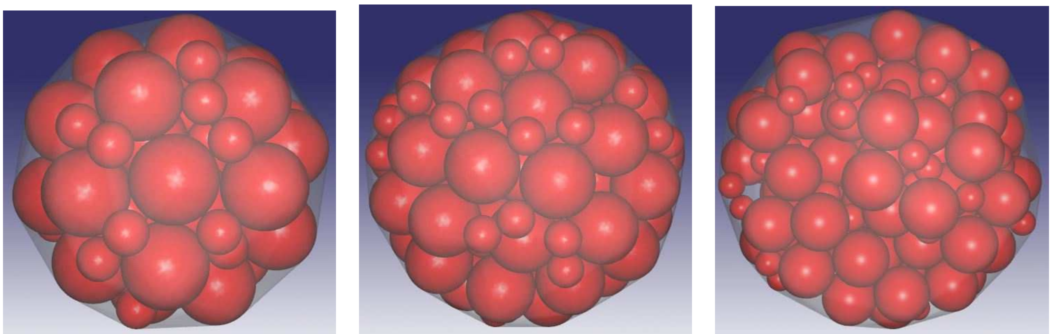

(a) 60 non-congruent spheres. (b) 120 non-congruent spheres. (c) 200 non-congruent spheres.

Fig. 9 Spherical arrangement of non-congruent spheres for two types of spheres, one half with radius $R = 1$ and the other half with radius $R = 1/2$.

The validity of Conjecture 1 is strengthened by large scale experiments for spheres for which we set the radii systematically in a slightly different way, which led to acceptable computing times of 24 h. Instance NC200b contains 200 non-congruent spheres with radii $R_i = 201 - i$. The resulting arrangement is shown in Figure 10.

Another interesting finding is the area ratio ρ_{a} of $A(\partial\mathcal{S})$ and the area of all spheres enclosed by $\mathcal{S}$. The greater the number of instances, the lower this ratio. Analytically, for large numbers n of spheres of radius R and volume utilization ρ_{v}, we would expect

$$\sum_i \frac{4}{3}\pi R^3 = \frac{4n}{3}\pi R^3 = \rho_{\mathrm{v}} V(\mathcal{S}) = \rho_{\mathrm{v}} \frac{4}{3}\pi r^3,$$

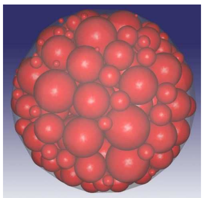

Fig. 10 Resulting arrangement of instance NC200b with 200 spheres with radius $R_i = 201 - i$ for sphere $i = 1, \ldots, 200$.

from which the radius r of the convex hull follows as

$$r = \left(\frac{n}{\rho_\mathrm{v}}\right)^{1/3} R.$$

Similarly, for $n/2$ spheres of radius R and $n/2$ spheres of radius $R/2$, we obtain

$$\frac{4n}{3}\pi R^3 \frac{1+2^{-3}}{2} = \rho_\mathrm{v}\frac{4}{3}\pi r^3,$$

and thus

$$r = \left(\frac{9}{16}\frac{n}{\rho_\mathrm{v}}\right)^{1/3} R.$$

This yields the area ratio

$$\rho_\mathrm{a} = \left(\frac{n}{\rho_\mathrm{v}}\right)^{2/3}\frac{1}{n} = \left(\frac{1}{\rho_\mathrm{v}}\right)^{2/3} n^{-1/3},$$

or

$$\rho_\mathrm{a} = \left(\frac{9}{16}\frac{n}{\rho_\mathrm{v}}\right)^{2/3} \Big/ \left(\frac{n}{2}(1+2^{-2})\right) = \frac{8}{5}\left(\frac{9}{16}\frac{1}{\rho_\mathrm{v}}\right)^{2/3} n^{-1/3},$$

respectively, *i.e.*, in both cases a slowly and monotonously decreasing function of n as displayed in Fig. 11. For NC190, *i.e.*, 95 spheres with radius $R = 1$ and 95 spheres with radius $R/2$, we obtain numerically

$$\rho_\mathrm{v} = \frac{\frac{4}{3}\pi(95 + 95/2^3)}{734.475} \simeq 0.60952,$$

and, finally,

$$\rho_\mathrm{a} = \frac{8}{5}\left(\frac{16}{9}\frac{\frac{4}{3}\pi(95+95/2^3)}{734.475}\right)^{-2/3} \cdot 190^{-1/3} \simeq 0.26381.$$

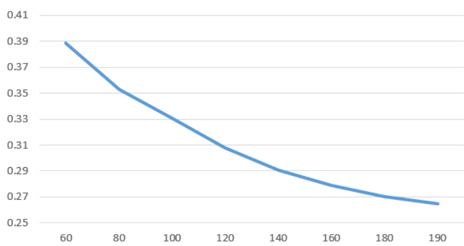

Fig. 11 Area ratio, ρ_a, of $A(\partial\mathcal{S})$ and the area of all spheres enclosed by $\mathcal{S}$ for instances NC60 to NC200.

4.3.3 Results for spheres in a rectangular solid

As in practice we often face the problem of packing items into a restricted space, we also conduct the study of packing spheres into a rectangular solid representing, for example, a container, the loading area of a truck, or a box. The resulting packing problem is similar to the 3D bin packing problem in which items of rectangular shape are arranged in a box (see [24]). Thus, we try to find an answer to the decision problem whether a given number of spheres (items) fit into a given rectangular solid. Similar to the 3D bin packing problem, finding an answer for this decision problem is NP-hard to solve.

Although we have to only slightly change the model formulation, the new problem statement significantly influences the resulting arrangement of spheres. On the one hand, as we now consider a restricted area in which the spheres can be placed, a given arrangement of spheres may be infeasible, as one or more spheres violate the bounds of a restricting border. On the other hand, a feasible arrangement of spheres, *i.e.*, all spheres fit into the rectangular solid, does not necessary lead to the property that as few as three spheres must touch each other.

In our computational study, we pack the eight non-congruent spheres of instance NC8 into a rectangular solid of the dimension $\mathbf{x}^{\mathrm{R}} := (10, 10, 8)^{\mathrm{T}}$, $\mathbf{x}^{\mathrm{R}} := (20, 6, 6)^{\mathrm{T}}$, and $\mathbf{x}^{\mathrm{R}} := (18, 6, 6)^{\mathrm{T}}$, respectively. This is accomplished by the additional inequalities (in coordinate framework 1)

$$x_{id}^{0} \leq x_{d}^{\mathrm{R}}; \quad \forall \{id\}.$$

The solution of the sphere packing is shown in Fig. 12.

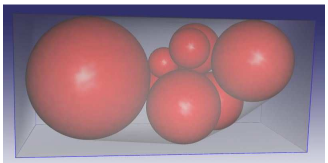

Fig. 12 The packing of instance NC8 into a rectangular solid of dimension $\mathbf{x}^{\mathrm{R}} := (10, 10, 8)^{\mathrm{T}}$, $\mathbf{x}^{\mathrm{R}} := (20, 6, 6)^{\mathrm{T}}$, and $\mathbf{x}^{\mathrm{R}} := (18, 6, 6)^{\mathrm{T}}$.

4.4 Experimental insights

Based on our analytical solutions for two to five spheres, as well as our experimental study, we summarize the following experimental insights:

1. We cannot close the gap between upper and lower bounds provided by `BARON`. Thus, in the sense of deterministic global optimization, we cannot be sure that we obtained the global minimum. However, for test cases with known analytic solutions, we observe $A^{\mathrm{gP}} \leq A \leq A^{\mathrm{sH}}$, where A is the area of according to the analytical solution, *i.e.*, the sum (2.12) is a lower bound for A. For 29 θ-circles the approximation error is less than 0.1%.
2. In solutions with less than five spheres, all spheres touch each other, *i.e.*, they are in *complete contact* and the non-overlap inequalities (2.8) are fulfilled as equalities for all sphere combinations.
3. For five spheres with radii $R_1 \geq R_2 \geq \ldots \geq R_5$, we observe that in the apparently optimal solutions, the first four spheres are in complete contact, and that spheres 1, 2, 3, and 5 are in complete contact.

5 Conclusions

This paper studies the problem of arranging spheres with possibly different radii such that the surface area of the boundary of the convex hull is minimized. To solve the problem, we have developed non-convex NLP models and provide interesting theoretical insights. Based on analytic solutions for up to five spheres, we have tuned the number of grid points as well as the numerical integration error. This enabled us to validate the NLP model and that it produces, at least for these cases, the global minimum. Moreover, we provide interesting insights into arrangement characteristics of minimal surface area convex hulls.

As the general problem is NP-hard to solve, we evaluate five algorithmic setups for solving the problem. Computationally, we are able to solve problems involving up to 200 spheres. By means of those experimental setups, we can support the conjecture that minimal surface area convex hulls of congruent spheres approach a sphere. Our experiments indicate that this also seems to hold for non-congruent spheres.

Acknowledgement

We thank Julius Näumann (Student, TU Darmstadt, Darmstadt, Germany) for producing the graphics software for this paper. Thanks are directed to Dr. Jens Schulz (Lufthansa Systems GmbH, Berlin, Germany), Prof. Dr. Julia Kallrath (Hochschule Darmstadt, Darmstadt, Germany), Julius Näumann, Dr. Fritz Näumann (Consultant, Weisenheim am Berg, Germany), and Dr. Wolfgang Heinecke (Edenkoben, Germany) for their careful reading of and feedback on the manuscript.

References

1. Bisschop, J., Meeraus, A.: On the Development of a General Algebraic Modeling System in a Strategic Planning Environment. In: Applications, *Mathematical Programming Studies*, vol. 20, pp. 1–29. Springer Berlin Heidelberg (1982)
2. Boissonnat, J.D., Cérézo, A., Devillers, O., Duquesne, J., Yvinec, M.: An Algorithm for Constructing the Convex Hull of a Set of Spheres in Dimension *d*. Computational Geometry **6**(2), 123 – 130 (1996)
3. Bussieck, M.R., Meeraus, A.: General Algebraic Modeling System (GAMS). In: J. Kallrath (ed.) Modeling Languages in Mathematical Optimization, *Applied Optimization*, vol. 88, pp. 137–157. Springer US (2004)
4. Bussieck, M.R., Meeraus, A.: Algebraic Modeling for IP and MIP (GAMS). In: Annals of Operations Research, vol. 149(1), special edition History of Integer Programming: Distinguished Personal Notes and Reminiscences, Guest Editors: Kurt Spielberg and Monique Guignard-Spielberg, pp. 49–56. Kluwer Academic Publishers-Plenum Publishers, Dordrecht, The Netherlands (2007)
5. Byungioo, K., Ku-Jin, K.: Computing the Convex Hull for a Set of Spheres on a GPU. In: Proceedings of the 11th ACM SIGGRAPH International Conference on Virtual-Reality Continuum and its Applications in Industry, p. 345 (2012)
6. Byungioo, K., Ku-Jin, K., Young J., K.: Approximating the Convex Hull for a Set of Spheres. KIPS Transactions on Computer and Communication Systems **3**(1), 1 – 6 (2014)
7. Chen, D.: Sphere Packing Problem. In: M.Y. Kao (ed.) Encyclopedia of Algorithms. Springer (2001)
8. Conway, J., Sloane, N., James, A.: Sphere Packings, Lattices, and Groups, vol. 2. Springer (1999)
9. Corporation, G.D.: General Algebraic Modeling System (GAMS) Release 24.9.2. Washington, DC, USA (2017). URL http://www.gams.com/
10. Costa, A., Hansen, P., Liberti, L.: On the Impact of Symmetry-breaking Constraints on Spatial Branch-and-Bound for Circle Packing in a Square. Discrete Applied Mathematics **161**(1-2), 96–106 (2013). DOI 10.1016/j.dam.2012.07.020
11. Devillers, O., Golin, M.J.: Incremental Algorithms for Finding the Convex Hulls of Circles and the Lower Envelopes of Parabolas. Inf. Process. Lett. **56**(3), 157–164 (1995). DOI 10.1016/0020-0190(95)00132-V
12. Hadwiger, H.: Die isoperimetrische Ungleichung im Raum. Elemente der Mathematik **3**, 25–38 (1948). URL http://eudml.org/doc/140476

13. Hifi, M., M'Hallah, R.: A Literature Review on Circle and Sphere Packing Problems: Models and Methodologies. Advances in Operations Research **2009**, 1–22 (2009)
14. Kallrath, J.: Cutting Circles and Polygons from Area-Minimizing Rectangles. Journal of Global Optimization **43**, 299–328 (2009)
15. Kallrath, J.: Polylithic Modeling and Solution Approaches Using Algebraic Modeling Systems. Optimization Letters **5**, 453–466 (2011). 10.1007/s11590-011-0320-4
16. Kallrath, J., Frey, M.T.: Packing Circles into Perimeter-Minimizing Convex Hulls. Journal of Global Optimization **submitted, revised version after 2nd review** (2018)
17. Kallrath, J., Milone, E.F.: Eclipsing Binary Stars: Modeling and Analysis. Springer, New York, 384 pages (1999)
18. Karavelas, M.I., Tzanaki, E.: Convex Hulls of Spheres and Convex Hulls of Convex Polytopes lying on Parallel Hyperplanes. In: Symposium on Computational Geometry, pp. 397–406. ACM (2011)
19. Li, S., Zhao, J., Lu, P., Xib, Y.: Maximum Packing Density of Basic 3D Objects. Chinese Science Bulletin **55**(2), 114–119 (2010)
20. MacLean, K.J.M.: A Geometric Analysis of the Platonic Solids and other Semi-Regular Polyhedra. Kenneth James Michael MacLean, Ann Arbor, MI, USA (2006)
21. Markót, M.C.: Interval Methods for Verifying Structural Optimality of Circle Packing Configurations in the Unit Square. J. Computational and Applied Mathematics **199**, 353–357 (2007)
22. Markót, M.C., Csendes, T.: A New Verified Optimization Technique for the "Packing Circles in a Unit Square" Problems. SIAM J. Optimization **16**, 193–219 (2005)
23. Marshall, G., Hudson, T.: Dense Binary Sphere Packings. Contributions to Algebra and Geometry **51**(2), 337 – 344 (2010)
24. Martello, S., Pisinger, D., Vigo, D.: The Three-Dimensional Bin Packing Problem. Operations Research **48**(2) (2000)
25. Rappaport, D.: Minimum Polygon Transversals of Line Segements. International Journal of Computational Geometry & Applications **5**(3) (1995)
26. Rogers, C.: The Packing of equal Spheres. In: Proceedings of the London Mathematical Society, vol. 3 (1958)
27. Tawarmalani, M., Sahinidis, N.V.: Convexification and Global Optimization in Continuous and Mixed-Integer Nonlinear Programming: Theory, Algorithms, Software, and Applications. Nonconvex Optimization And Its Applications Series. Kluwer Academic Publishers, Dordrecht, The Netherlands (2002)
28. Wilson, R.E., Devinney, E.J.: Realization of Accurate Close-Binary Light Curves: Application to MR Cygni. The Astrophysical Journal **166**, 605–619 (1971)
29. Zong, C.: Strange Phenomena in Convex and Discrete Geometry. Springer (1996)
30. Zong, C.: Sphere Packings, vol. 1. Springer, New York (1999)

A Notation

We start with the symbols introduced in the derivation of the model; they are not used in the NLP model directly.

$A(\partial\mathcal{S})$	surface area of the boundary $\partial\mathcal{S}$ of the convex hull $\mathcal{S}$ enclosing the spheres.
$A_{4,2x2}$	total surface of convex hull ∂S for four congruent spheres in the plane.
A_n^s	area of the convex hull for n spheres.
A_c	area of a cube with pre-specified volume.
A_s	area of a sphere with pre-specified volume.
A^{gP}	approximate value of the area of $\partial\mathcal{S}$ derived from the QuickHull algorithm exploiting the variables $\mathbf{x}_{\theta\varphi}$ computed by the NLP model.
A^{sL}	approximate value of the area of $\partial\mathcal{S}$ derived from the QuickHull algorithm applied to points resulting from a discretization of the surfaces of all spheres (coarse grid).
A^{sH}	approximate value of the area of $\partial\mathcal{S}$ derived from the QuickHull algorithm applied to points resulting from a discretization of the surfaces of all spheres (fine grid).
$A_n^{\mathbf{th}}$	Total surface of ∂S for n spheres.
C_4^{2x2}	planar, square-arrangement of four spheres.
$\mathbf{m}_{\theta\varphi}$	direction vectors over the unit sphere in spherical coordinates $\theta \in [0,\pi]$ and $\varphi \in [0, 2\pi]$.
n	the number of spheres to be placed.
r	radius of a volume-equivalent sphere.
$\mathcal{S}$	the convex hull hosting all spheres.
$\partial\mathcal{S}$	the boundary of the convex hull hosting all spheres.
$V(\mathcal{S})$	the volume of the convex hull $\mathcal{S}$ enclosing the spheres.
V^{gP}	approximate value of the volume of $\mathcal{S}$ derived from the QuickHull algorithm exploiting the variables $\mathbf{x}_{\theta\varphi}$ computed by the NLP model.

V^{sL} approximate value of the volume of $\mathcal{S}$ derived from the QuickHull algorithm applied to points resulting from a discretization of the surfaces of all spheres (coarse grid).

V^{sH} approximate value of the volume of $\mathcal{S}$ derived from the QuickHull algorithm applied to points resulting from a discretization of the surfaces of all spheres (fine grid).

V_n^s volume of the sausage configuration with n spheres.

$V_n^{\mathbf{th}}$ total volume of n spheres.

β dihedral angle formed by the intersection of two planes of the tetrahedron.

γ inner angle of a spherical triangle used to derive the solid angle contributed by the spheres in a tetrahedron-arrangement.

Δ value of the distance correction term.

ϵ a small positive number.

ρ the ratio R_2/R_1.

The symbols used in the NLP model are summarized in the following subsections.

A.1 Indices and Sets

$d \in \{1, 2, 3\}$ index for the dimension; $d = 1$ represents the x-coordinate, y-coordinate, and $d = 3$ the z-coordinate.

$i \in \mathcal{I} := \{1, \ldots, n\}$ objects (spheres) to be packed or arranged.

$\mu \in 1, \ldots, N_\theta$ index to refer to latitude circles θ_μ on the unit sphere.

$\nu \in 1, \ldots, N_\varphi(\theta_\mu)$ index to refer to grid points on a latitude circle on the unit sphere.

A.2 Data

D_{ij} distance of the centers of sphere i and sphere j.

R_i radius of sphere i to be placed.

A.3 Decision Variables

$\mathbf{n}_{\theta\varphi}$ normal vector at grid point $\mathbf{x}_{\theta\varphi}$ of the boundary of the convex hull.

n^{D} distance-to-origin of the tangential plane at grid point $\mathbf{x}_{\theta\varphi}$ of the boundary of the convex hull.

$r_{\mu\nu}$ radial distance of a grid point of the boundary of the convex hull to the center-of-centers, $\mathbf{x}_{\mathrm{c}}$.

$x_{d\mu\nu}$ d-coordinate of a grid point of the boundary of the convex hull; this variable is synonym to $\mathbf{x}_{\theta\varphi}$, or $\mathbf{x}_{\theta_\mu\varphi_\nu}$.

x_{id}^0 d-coordinate of the center vector of sphere i to be placed

x_{cd} d-coordinate of the average radius-weighted centers of sphere

$\mathbf{x}_{\theta\varphi}$ in the NLP model, we denote this variable as $x_{d\mu\nu}$.

$x^{\mathbf{R}}$ the size of the rectangular box; only needed in P2, or when fitting the convex hull into the rectangular solid.

$x_d^{\mathbf{R}}$ d-coordinate of x^{R}, the size of the rectangular solid.

B Detailed Derivations

In this section we provide various derivations in detail.

B.1 Analytic Solutions – Detailed Derivations

B.1.1 Two Spheres

Let us now consider two spheres with radii R_1 and R_2, $R_1 \geq R_2$ arranged such that the distance of their centers is $d \geq R_1 + R_2$; note that in this section d does not refer to the dimension. From Fig. 3 we derive

$$m = \sqrt{d^2 - (R_1 - R_2)^2} = R_1\sqrt{(1 + \delta + \varepsilon)^2 - (1 - \delta)^2} = R_1\sqrt{4\delta + 2\varepsilon + 2\delta\varepsilon + \varepsilon^2}.$$

Cosine law plus diagonal in Fig. 3 yields

$$m^2 + R_2^2 = R_1^2 + d^2 - 2R_1 d \cos\alpha_1$$

$$
\begin{aligned}
d^2-(R_1-R_2)^2+R_2^2 &= R_1^2+d^2-2R_1 d\cos\alpha_1\\
-(R_1-R_2)^2+R_2^2 &= R_1^2-2R_1 d\cos\alpha_1=(R_1-2d\cos\alpha_1)\,R_1\\
\cos\alpha_1=\frac{R_1^2+(R_1-R_2)^2-R_2^2}{2R_1 d} &= \frac{2R_1^2-2R_1R_2}{2R_1 d}=\frac{R_1-R_2}{d}=\frac{1-\delta}{1+\delta+\varepsilon}
\end{aligned}
$$

with the abbreviations

$$\delta:=\frac{R_2}{R_1},\quad \varepsilon:=\frac{d-(R_1+R_2)}{R_1}.$$

This enables us to derive the relations

$$\sin^2\alpha_1=1-\cos^2\alpha_1=1-\left(\frac{1-\delta}{1+\delta+\varepsilon}\right)^2=\frac{(1+\delta+\varepsilon)^2-(1-\delta)^2}{(1+\delta+\varepsilon)^2}=\frac{4\delta+2\varepsilon+2\delta\varepsilon+\varepsilon^2}{(1+\delta+\varepsilon)^2}$$

$$\sin\alpha_1=\frac{\sqrt{4\delta+2\varepsilon+2\delta\varepsilon+\varepsilon^2}}{1+\delta+\varepsilon}\longrightarrow\frac{2\sqrt{\delta}}{1+\delta}$$

and

$$
\begin{aligned}
1+\cos\alpha_1 &= 1+\frac{R_1-R_2}{d}=1+\frac{1-\delta}{1+\delta+\varepsilon}=\frac{2+\varepsilon}{1+\delta+\varepsilon}\longrightarrow\frac{2}{1+\delta}\\
1-\cos\alpha_1 &= 1-\frac{R_1-R_2}{d}=1-\frac{1-\delta}{1+\delta+\varepsilon}=\frac{2\delta+\varepsilon}{1+\delta+\varepsilon}\longrightarrow\frac{2\delta}{1+\delta}.
\end{aligned}
$$

From the segment angles

$$\alpha_1,\quad \alpha_2=\pi-\alpha_1$$

we derive the radii r_i of the truncated cone on the side of sphere i

$$r_i=R_i\sin\alpha_i,$$

the height h of the truncated cone

$$h=\sqrt{m^2-(r_1-r_2)^2},$$

its area M

$$M\ =\pi\,(r_1+r_2)\,m,$$

the heights h_i of the segments of the spheres

$$h_i=R_i\,[1-\cos\alpha_1]=R_i\left[1-\frac{1-\delta}{1+\delta+\varepsilon}\right],$$

and finally the surface areas A_i of the segments of the spheres

$$A_i\ =2\pi R_i h_i=2\pi R_i^2\,[1-\cos\alpha_1]\,.$$

Note that for both spheres the relevant angle for computing the segment areas is α_1. Finally, we obtain as the surface area, A, of the boundary of the convex hull

$$
\begin{aligned}
A &= \left[4\pi R_1^2-A_1\right]+M+A_2\\
&= \pi\left[4R_1^2+2(R_2h_2-R_1h_1)+(r_1+r_2)\,m\right]\\
&= 2\pi\left[2R_1^2+R_2^2(1-\cos\alpha_1)-R_1^2(1-\cos\alpha_1)+(R_1\sin\alpha_1+R_2\sin\alpha_2)\,\frac{m}{2}\right]\\
&= 2\pi\left[2R_1^2+R_2^2(1-\cos\alpha_1)-R_1^2(1-\cos\alpha_1)+(R_1\sin\alpha_1+R_2\sin\alpha_1)\,\frac{m}{2}\right]\\
&= 2\pi\left[2R_1^2+R_2^2(1-\cos\alpha_1)-R_1^2(1-\cos\alpha_1)+(R_1+R_2)\,\frac{m}{2}\sin\alpha_1\right]\\
&= 2\pi R_1^2\left[2+\delta^2\frac{2\delta+\varepsilon}{1+\delta+\varepsilon}-\frac{2\delta+\varepsilon}{1+\delta+\varepsilon}+(1+\delta)\frac{4\delta+2\varepsilon+2\delta\varepsilon+\varepsilon^2}{2\,(1+\delta+\varepsilon)}\right]\\
&= \pi R_1^2\left[\frac{4(1+\delta+\varepsilon)+2\delta^2\,(2\delta+\varepsilon)-2(2\delta+\varepsilon)+(1+\delta)\left(4\delta+2\varepsilon+2\delta\varepsilon+\varepsilon^2\right)}{1+\delta+\varepsilon}\right]\\
&= 4\pi R_1^2\frac{1}{1+\delta+\varepsilon}\left[1+\delta+\delta^2+\delta^3+\varepsilon+\delta\varepsilon+\frac{1}{4}\varepsilon^2+\frac{1}{4}\delta\varepsilon^2+\delta^2\varepsilon\right]\\
&= 4\pi R_1^2\left[1+\delta^2+\varepsilon+\frac{1}{4}\varepsilon^2+\frac{1}{1+\delta+\varepsilon}\left(\varepsilon+\frac{1}{4}\varepsilon^2+(\varepsilon+1)\left(-\varepsilon-\frac{1}{4}\varepsilon^2-1\right)+1\right)\right]\\
&= 4\pi R_1^2\left[1+\delta^2+\frac{\varepsilon}{4}\frac{4\delta+\varepsilon+\delta\varepsilon}{1+\delta+\varepsilon}\right].
\end{aligned}
$$

For small values of ε, the non-negative *detached-correction* term

$$\varDelta := \frac{\varepsilon}{4}\frac{4\delta+\varepsilon+\delta\varepsilon}{1+\delta+\varepsilon}$$

approaches zero, while for $\varepsilon \to +\infty$ the term diverges to $+\infty$. As $\varDelta \geq 0$, for $\varepsilon = 0$, $A(\partial\mathcal{S})$ takes its minimal value

$$A_{2c} = 4\pi R_1^2\left[1+\delta^2\right] = 4\pi R_1^2 + 4\pi R_2^2.$$

This proves our intuitive view that we get minimal area $\partial\mathcal{S}$ when the two spheres touch each other, *i.e.*, they are in contact. Note that for two equal spheres, the area contributed by each sphere is half of the surface area of each sphere. To complete the picture, we provide the solid angles $\tilde{\alpha}_1$ and $\tilde{\alpha}_2$ the spheres contribute to $\partial\mathcal{S}$

$$\begin{aligned}\tilde{\alpha}_1 &= 2\cdot(2\pi-2\alpha_1)\\ \tilde{\alpha}_2 &= 2\cdot 2\alpha_1,\end{aligned}$$

and thus for the sum of the solid angles

$$\tilde{\alpha}_1+\tilde{\alpha}_2 = 4\pi.$$

Note that this is true for any two non-overlapping spheres with arbitrary radii and we have not assumed that the spheres touch each other.

B.1.2 Three Spheres

Here, we derive the center coordinates of three spheres with radii $R_1 \geq R_2 \geq R_3$. We exploit from the result of two spheres that minimal $A(\partial\mathcal{S})$ is obtained when the three spheres are in contact, *i.e.*, the center coordinates are subject to the simultaneous conditions

$$\left(\mathbf{x}^0_{i_1}-\mathbf{x}^0_{i_2}\right)^2 = \left(R_{i_1}+R_{i_2}\right)^2, \quad \forall\{(i_1 i_2) = (1,2),(1,3),(2,3)\}.$$

Without loss of generality, we fix the z-coordinate $x_{13}, x_{23}, x_{33} = 0$ for all spheres, and the y-coordinate $x_{12}, x_{22} = 0$ for sphere 1 and 2. We further fix $x_{11} = 0$, *i.e.*, spheres 1 is placed at $(0,0,0)$. This leaves us with three unknown variables (x_{21}, x_{31}, x_{22}) to be obtained from

$$\begin{aligned}(x_{21}-x_{11})^2 &= (R_1+R_2)^2\\ x_{21} &= R_1+R_2 = R_1\,(1+\delta)\,, \quad \delta := R_2/R_1\end{aligned}$$

and

$$\begin{aligned}(x_{31}-x_{11})^2+(x_{32}-x_{12})^2 &= (R_1+R_3)^2\\ x_{31}^2+x_{32}^2 &= (R_1+R_3)^2 = R_1^2\left(1+\nu^2\right), \quad \nu := R_3/R_1\end{aligned}$$

and

$$\begin{aligned}(x_{31}-x_{21})^2+(x_{32}-x_{22})^2 &= (R_2+R_3)^2\\ (x_{31}-R_1-R_2)^2+x_{32}^2 &= (R_2+R_3)^2 = R_1^2\left(\delta^2+\nu^2\right).\end{aligned}$$

From

$$\begin{aligned}x_{31}^2+x_{32}^2 &= (R_1+R_3)^2\\ (x_{31}-R_1-R_2)^2+x_{32}^2 &= (R_2+R_3)^2\end{aligned}$$

or

$$x_{31}^2-(x_{31}-R_1-R_2)^2 = (R_1+R_3)^2-(R_2+R_3)^2$$

or

$$\begin{aligned}u^2-(u-R_1-R_2)^2 &= (R_1+R_3)^2-(R_2+R_3)^2\\ 2uR_1+2uR_2-2R_1R_2-R_1^2-R_2^2 &= 2R_1R_3-2R_2R_3+R_1^2-R_2^2\end{aligned}$$

and thus

$$x_{31} = u = \frac{R_1R_2+R_1R_3-R_2R_3+R_1^2}{R_1+R_2},$$

from which we get

$$x_{32}^2 = (R_1 + R_3)^2 - \left(\frac{R_1R_2 + R_1R_3 - R_2R_3 + R_1^2}{R_1 + R_2} \right)^2$$
$$= 4\,(R_1 + R_2)^{-2}\,(R_1 + R_2 + R_3)\,R_1R_2R_3$$

or

$$x_{32} = \frac{2}{R_1 + R_2} \sqrt{(R_1 + R_2 + R_3)\,R_1R_2R_3}.$$

If we want to place all spheres in the first octant, we just transform all coordinates to (R_1, R_1, R_1) and obtain the center coordinates of the spheres as

$$(x_{11}, x_{12}, x_{13}) = R_1(1, 1, 1),$$

$$(x_{21}, x_{22}, x_{23}) = R_1(2 + \delta, 1, 1),$$

$$(x_{31}, x_{32}, x_{33}) = \left(R_1 + \frac{R_1R_2 + R_1R_3 - R_2R_3 + R_1^2}{R_1 + R_2}, R_1 + \frac{2}{R_1 + R_2} \sqrt{(R_1 + R_2 + R_3)\,R_1R_2R_3}, R_1 \right).$$

B.2 Proofs

B.2.1 The sum of the sector angles

We show that a) for n spheres with arbitrary radius R, the solid angles contributed by the spheres to $\partial\mathcal{S}$ add up to 4π, and b) that for n congruent spheres with radius R, the surface areas of all partial sphere facets contributed to $\partial\mathcal{S}$ add up to the surface of the full sphere, *i.e.*, $4\pi R^2$. For $n = 1$, the result is obvious as the convex hull is identical to the sphere itself. For $n = 2$, both statements a) and b) have been proven in Appendix B.1.1. For $n > 2$, the proof for a) is a generalization of the proof developed in [16] to prove the analogue property in the 2D case. As we consider here the 3D case, we basically replace *angles* by *solid angles*.

Consider any set of spheres with arbitrary radii R_i enclosed by their convex hull $\mathcal{S}$. Note, we do not require that either $V(\mathcal{S})$ nor $A(\partial\mathcal{S})$ is minimal. The sum of the solid angles $\tilde{\alpha}_i$ of the spherical facets contributing to $\partial\mathcal{S}$ equals to 4π steradians. Before we conduct the general proof 3), we prove the statement for planar (1) and special symmetric configurations (2).

Proof: 1) *Planar configurations*: We prove the statement for planar configurations by projecting the spheres onto the $x - y-$plane, which enables us to exploit the theorem in the 2D case of [16], yielding the angles α_i in 2D adding up to 2π, *i.e.*,

$$\sum_i \alpha_i = 2\pi.$$

Therefore, we obtain for the solid angles $\tilde{\alpha}_i$

$$\tilde{\alpha}_i = \int_0^{\pi} \int_0^{\alpha_i} \sin\theta \mathrm{d}\varphi \mathrm{d}\theta = 2\alpha_i.$$

Thus, the sum of all solid angles $\tilde{\alpha}_i$ adds up to

$$\sum_i \tilde{\alpha}_i = \sum_i (2\alpha_i) = 4\pi,$$

which implies that for spheres with equal radius R, we obtain a surface area of $4\pi R^2$, *i.e.*, the area of a full sphere which proves the statement for planar configurations (*q.e.d.*).

2) *Symmetric configurations*: For symmetric configurations in which all spheres have the same radius R, for instance, $\mathcal{C}_3^{\mathrm{p}}$, $\mathcal{C}_4^{2\mathrm{x}2}$, or $\mathcal{C}_4^{\mathrm{t}}$, we prove the statement by exploiting the shadow property briefly described in Section 2.1. Due to this restrictions (symmetry and equal radius), each sphere contributes the same area to $\partial\mathcal{S}$. Let us consider n spheres with equal radius R, surface area A_s touching and contributing to $\partial\mathcal{S}$, and denote the area contributed by A_i. Due to the symmetry we have

$$A_i = \frac{1}{n} A_*, \quad \forall i$$

with some reference area A_*. If we can show $A_* = A_s$, we have shown that the area contributions of the n spheres to $\partial\mathcal{S}$ are A_s. As shown in detail in Appendix B.1.1, the statement is true for $n = 2$.

Now consider configuration $\mathcal{C}_3^{\mathrm{p}}$ and sphere 1 to begin with. Due to the shadow property, we can first eliminate half of the surface points of sphere 1 due the presence and shining of sphere 2 onto sphere 1. Sphere 3 also eliminates half the surface points of sphere 1, but there is an overlap with the eliminated points from sphere 2. This is illustrated in Fig. 13. Projected on the $x-y-$plane, we obtain an angle α of $120°$, leading to a third of the surface area A_s of sphere 1. Symmetry implies the same for spheres 2 and 3. Note that the conversion from angles to solid angles for these planar configurations follows along the lines of the proof in part 1) above (*q.e.d.*). For configuration $\mathcal{C}_4^{2\times2}$ the same chain of arguments leads for sphere 1 with shining from sphere 2 and 4 to an

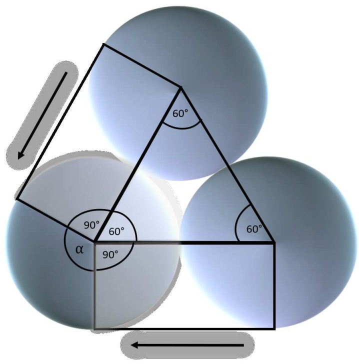

Fig. 13 The shadow property. Spheres 2 (lower right) and sphere 3 (upper level) shine onto sphere 1. That surface part of sphere 1 which receives shining light from both is brighter than those parts receiving only light from one sphere, and that part which does not receive light from either sphere remains dark and establishes a part of $\partial\mathcal{S}$.

angle of $\alpha = 90$. Thus, following along the lines of part 1) above, a quarter of the surface area of sphere 1 (*q.e.d.*).

Configuration $\mathcal{C}_4^{\mathrm{t}}$ is an extension of $\mathcal{C}_3^{\mathrm{p}}$, but sphere 4 above the three spheres of $\mathcal{C}_3^{\mathrm{p}}$ leaves only 3/4 of this third of surface of the spheres on the bottom level, *i.e.*, a quarter of the surface. To illustrate this, we have plotted the contributions of the spheres to $\partial\mathcal{S}$ in blue (Figure 14) (a). Each sphere contributes an equilateral spherical triangle of side length $s = 180 - \beta$ and inner angle γ of $120°$, or $2/3\pi$, in radian. Thus, according to spherical trigonometry, the area A_Δ of this equilateral spherical triangle is

$$A_\Delta = 3\gamma - \pi = \pi,$$

which is a quarter of the area of a unit sphere (*q.e.d.*).

3) *Non-planar configurations* (n spheres with arbitrary radii): To begin with the proof, let us inspect Figure 14 (b) and (c) displaying highlighting the parts of the spheres contributing to ∂S in the solution for instance NC5 and NC6.

The spheres contribute spherical polygons with k vertices to $\partial\mathcal{S}$ formed by k arcs of great circles. Spherical equilateral triangles as for $\mathcal{C}_4^{\mathrm{t}}$ mean a special case. If sphere i does not contribute to $\partial\mathcal{S}$, we set $\tilde{\alpha}_i = 0$. Now, we talk only about spheres contributing to $\partial\mathcal{S}$. The spheres contributing to $\partial\mathcal{S}$ define a direction of $\partial\mathcal{S}$ to the next adjacent sphere contributing to $\partial\mathcal{S}$. The number of k_i of a particular sphere i indicates the number of spheres adjacent to sphere i contributing to $\partial\mathcal{S}$. Adjacent, contributing spheres i and j are connected by a partial truncated cone with limiting arc $\mathcal{A}_i$ on sphere i and arc $\mathcal{A}_j$ on sphere j. Note that the arcs $\mathcal{A}_i$ and $\mathcal{A}_j$ have the same shape and orientation, *i.e.*, they are parallel in the following sense: If we re-scale both spheres to the same target radius R, for instance, to the larger of both radii, cut off the truncated cone, discard the triangles, and perform a parallel, orientation-conserving shift of $\mathcal{A}_j$ along the center-line of the connecting partial truncated cone towards $\mathcal{A}_i$, both arcs match precisely, *i.e.*, they fit in both a) shape and curvature as they belong to the same great circle of radius R, and b) in the size or length as re-scaling transforms the truncated cone into a cylinder. If this was not the case then there must be another sphere between i and j due to the convexity property of $\partial\mathcal{S}$. Therefore, we can add the solid angles $\tilde{\alpha}_i$ and $\tilde{\alpha}_j$, and obtain, for the composite (non-convex) spherical polygon, the composite solid angle $\tilde{\alpha}_i + \tilde{\alpha}_j$.

Note that neither the parallel shifts nor the scaling change the individual solid angles. Note further that now the spheres may overlap. However, this is not relevant as we are only interested in edge-matching the spherical polygons. If we apply this procedure now to all k_i arcs of sphere i, and similarly to all other spheres and their arcs, we cover the sphere of target radius R completely by spherical polygons having matching arcs, and thus $\sum_i \tilde{\alpha}_i = 4\pi$ (q.e.d).

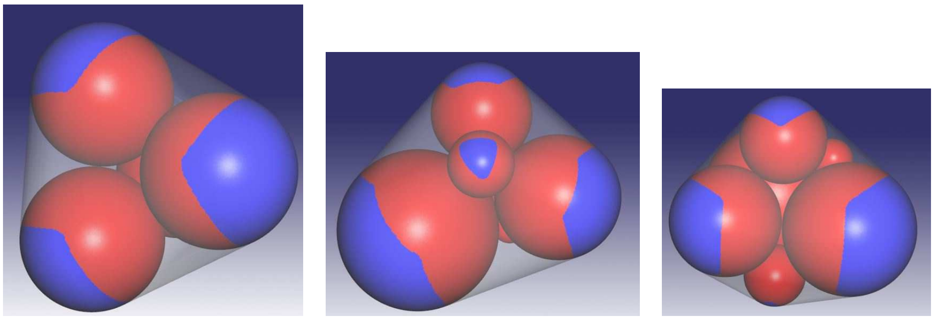

(a) The blue partial spheres contribute to ∂S an equilateral spherical triangle of side length $s = 180 - \beta$ and inner angle γ of 120°, or $2/3\pi$, in radian.

(b) The computed configuration of NC5, and its convex hull. We can recognize that spheres contribute spherical polygons (in blue) with up to four arcs to $\partial \mathcal{S}$. Note that the limiting arcs of the truncated cones connecting adjacent spheres have the same orientation.

(c) The computed configuration of NC6 ($n = 6$ spheres), and its convex hull. We can recognize that spheres contribute spherical polygons (in blue) with up to five arcs to $\partial \mathcal{S}$. Note that the limiting arcs of the truncated cones connecting adjacent spheres have the same orientation.

Fig. 14 The blue parts (spherical polygons) of the spheres contribute to ∂S. For arrangements with n spheres, the spherical polygons can have $k \leq n-1$ vertices or arcs, respectively. The arcs are parts of great circles.

In other words, we reduce $\partial \mathcal{S}$ to its scaled contributions from spherical facets with the connecting cones or triangles eliminated, and thus finally obtain a complete sphere. If, in the beginning, we had n spheres with equal radius R, the area of the all spherical polygons adds up to $4\pi R^2$ (q.e.d).

Remark: We could also consider the reverse procedure, *i.e.*, take a sphere, break its surface into spherical polygons, re-scale and move them apart performing parallel shifts until spheres do not overlap anymore, and construct the convex hull of these sphere arrangement.